Experimental and numerical study of dynamic regimes in a discrete sine-Gordon lattice

A. V. Ustinov,* M. Cirillo, Britt H. Larsen,† V. A. Oboznov,‡ P. Carelli,§ and G. Rotoli§
Dipartimento di Fisica, Universitá di Roma "Tor Vergata," I-00133 Roma, Italy
(Received 18 July 1994)

We investigate fluxon dynamics in underdamped one-dimensional parallel arrays of small Josephson tunnel junctions. The current-voltage characteristics of the arrays show various resonant steps depending upon the temperature of the sample and the externally applied magnetic field. Experimental results on fluxon propagation in arrays are compared with that for continuous Josephson transmission lines fabricated on the same chip. By modeling fluxon dynamic states in a one-dimensional array as a propagation of kinks in a discrete sine-Gordon lattice, we find consistency between numerical results and the experimental data. This consistency indicates that the concept of fluxons as moving relativistic particles can be still used even for strongly discrete lines. However, two important classes of phenomena are found which do not have any counterparts in the continuum case. These are concerned with the data that we obtain in the short-wavelength limit (determined by line discreteness) and with damping requirements that are necessary in order to stabilize kink propagation.

I. INTRODUCTION

The *continuum* perturbed sine-Gordon equation (PSGE) is known to be a model for a long Josephson junction[1] where a single magnetic flux quantum (fluxon) is a soliton-type solution of the equation. Fluxon dynamics in long Josephson junctions has been investigated in great detail during the last decade using as a solid theoretical background the perturbation theory by McLaughlin and Scott[3] based on the integrability of the continuum sine-Gordon equation. This theory describes fluxon dynamics in real junctions under various bias current conditions and structural perturbations. Thus, it has been possible to verify analytically or in numerical simulations many experimental features of long Josephson junctions and their mechanical analogs.[2]

One-dimensional (1D) parallel biased arrays of small Josephson junctions represent an experimental realization of the spatially *discrete* sine-Gordon lattice (also known as the Frenkel-Kontorova model). Magnetic flux dynamics in 1D arrays can be modeled by the discrete version of the sine-Gordon equation which is known to be nonintegrable. Although the discrete case is much simpler for numerical studies, this regrettable fact was understood a long time ago and it represented perhaps one of the reasons for which very few experiments have been performed in this field. Peyrard and Kruskal[4] pointed out that, even with large discreteness, the dynamics of a localized nonlinear kink in the sine-Gordon lattice may exhibit some features of solitonic nature (motion through the lattice with a negligible radiation) very close to the properties of the continuum sine-Gordon solitons. Thus, it becomes interesting to investigate parallels and differences in nonlinear kink propagation for the continuum and the discrete sine-Gordon systems.

Recently, experimentally measurable features in the dynamical behavior of *underdamped* 1D Josephson junction arrays have been studied in numerical simulations.[5,6] Propagation of fluxons through the underdamped 1D Josephson junction array with small discreteness should be evident because of the appearance of current singularities on the current-voltage characteristics (I-V curve) of the array. This phenomenon is analogous to the effects generated by fluxon motion in long quasi-one-dimensional Josephson junctions. Depending on the applied external magnetic field H, one may expect to observe the so-called zero-field steps (ZFS's), Fiske steps (FS's), and flux-flow steps (FFS's) (Ref. 1) in the I-V curves of the 1D arrays. If the discreteness of the array becomes larger, deviations from the continuum case are expected to appear. Recently, van der Zant *et al.*[7] performed experimental and analytical investigation of *linear* Fiske modes in short 1D arrays with moderate discreteness. Propagation of a single fluxon (a *nonlinear* kink) in the discrete limit has not been studied experimentally so far.

Experimental investigation of 1D arrays is a relevant issue in superconducting electronics because discretized Josephson transmission lines are the basis of the so-called phase-mode logic.[8] One of the advantages of such lines is that their inductance by capacitance product per unit length is smaller than that of a long Josephson junction. Due to this fact the maximum velocity of electromagnetic wave propagation in a transmission line (so-called Swihart velocity) is higher than in the continuum case. This factor increases the operation frequency of the discrete array with respect to the continuum long Josephson junction. Fluxon propagation in parallel arrays of superconducting quantum interference devices (SQUID's) is also the principle of operation of the rapid single flux quantum (RSFQ) circuits.[9] RSFQ devices use resistively shunted small Josephson junctions

which provide substantial damping, thus placing these circuits on the border between the overdamped and the underdamped limits. Static properties of parallel SQUID arrays [also called superconducting quantum interferometer gratings (SQUIG's)] have recently been studied numerically[10] with the aim of improving the single-loop SQUID characteristics needed for the magnetometry. Recently discrete arrays of *overdamped* Josephson junctions have gained interest after flux-flow devices were built from high-T_c superconducting films.[11] A flux-flow device consists of a row of weakened superconducting bridges as suggested by Likharev.[12] In the overdamped limit, flux flow in discrete arrays has been studied experimentally[13] and numerically.[14]

In this paper we study experimentally the fluxon dynamic regimes in 1D arrays of small underdamped tunnel Josephson junctions and compare the experimental results with numerical simulations based on the discrete sine-Gordon model. We have measured the *I-V* characteristics of 10- and 20-junction arrays as a function of the external magnetic field H at several different temperatures in order to vary the damping and the effective discreteness in the arrays. For what concerns the simulations we concentrated on the zero-field regimes and their interpretation based on the discrete sine-Gordon model. The paper is structured as follows: In the next section we present measuring techniques and experimental data. Section III describes the theoretical model and the results of numerical simulations. In Sec. IV we discuss and compare numerical data and experimental results. Finally, Sec. V summarizes the paper.

II. EXPERIMENTAL RESULTS

For the problem which we study here, the appropriate choice of the array geometry and the junction parameters is essential for an adequate comparison between theory and experiments. We designed the samples in order to get the discreteness parameter $a = \beta_L{}^{1/2} = (2\pi L_0 I_c/\Phi_0)^{1/2}$ of the order of unity at low temperatures. Here L_0 is the inductance of a single cell of the array, I_c is the critical current of each junction, and $\Phi_0 = 2.07\times10^{-15}$ Wb is the magnetic flux quantum. We used the simple linear geometry sketched in Fig. 1(a) with the number of junctions equal to 10 or 20 in different arrays. The choice of the number of junctions has been made keeping in mind that the usage of a very large N should lead to discreteness-induced resonances[6] in the *I-V* curve very closely spaced in voltage, thus making difficult their experimental investigation. On the other side, N has been taken to be not too small in order to realize the fluxon propagation regimes.

A. Samples and setup

Measurements were performed on parallel arrays of small niobium-lead tunnel Josephson junctions. Nb films with a thickness of 200 nm served as the base electrode; the tunnel barrier, grown by plasma oxidation of Nb, was covered by a 350-nm-thick Pb top electrode. The junctions in the arrays had an area of about 7 μm^2 and were connected by $5\times8\,\mu m^2$ superconducting loops. Every chip contained a 150-μm-long 10-junction array, a 300-μm-long 20-junction array, and two long junctions with dimensions in the plane of 4 μm$\times$100 μm. Technological details of the sample fabrication are described elsewhere.[15] The samples were surrounded by a cryoperm shield with a residual field inside it of about 15 mOe. The magnetic field perpendicular to the substrate was applied by a solenoid located inside the cryoperm shield. The sample was immersed directly in liquid helium or kept in gas above the liquid surface and its temperature

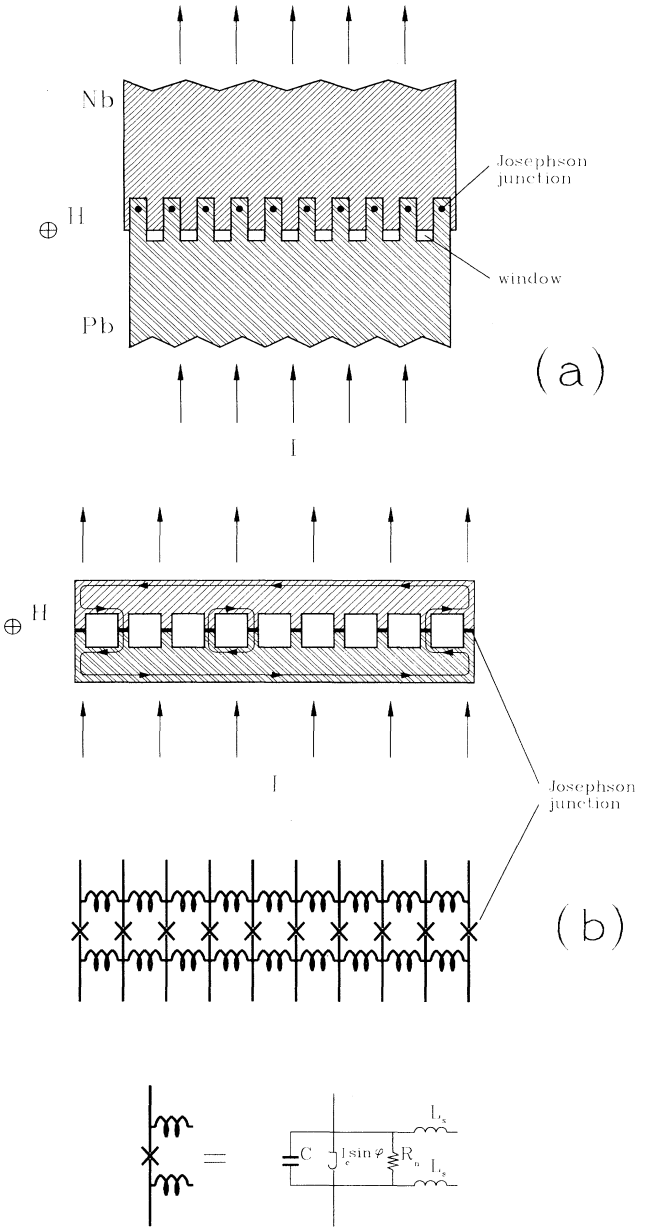

FIG. 1. (a) A sketch of the experimentally studied 1D Josephson junction array geometry. (b) Equivalent circuit used as a model for the 1D array ($L_s = L_0/2$).

was monitored by a silicon diode placed in close thermal contact with it. The *I-V* curves were recorded on a storage oscilloscope. The current to the sample was supplied by a battery-powered current source.

For long junctions from the same chip the following parameters were estimated from measured characteristics of our chips at 4.2 K: the critical current density $j_c = 160\ \mathrm{A/cm^2}$, the Josephson penetration depth $\lambda_J = 30\ \mu\mathrm{m}$, the Swihart velocity $\bar{c}_{\mathrm{LJJ}} = 0.05\, c_0$, where c_0 is the velocity of light in vacuum, and the capacitance per area for the junction, $C_s = 2.3\,\mu\mathrm{F/cm^2}$. At 4.2 K the normal resistance of the 10-junction array was measured to be $R_n = 3.6\,\Omega$. For the 20-junction array the normal resistance was $R_n = 1.8\,\Omega$. As expected for an array consisting of identical small junctions, the normal resistance R_n scales with the number of junctions.

B. Static properties: $I_c(H)$ dependence

For the 10-junction array the dependence of the critical current I_c on the applied magnetic field H measured at two different temperatures $T = 4.2$ K (a) and $T = 6.9$ K (b) is shown in Fig. 2. The $I_c(H)$ curves are appropriately symmetric with respect to $H = 0$ (the offset due to the residual field of about 15 mOe has been subtracted in the horizontal scale) and present a number of maxima in I_c spaced by roughly equal H intervals whose value stands around $H_1 = 28$ mOe . As expected for the multicontact SQUID characteristics, at each maximum the critical current I_c approximately reaches its value at zero field. These maxima of I_c correspond to the field values $H_m = m\Phi_0/S$ where the average magnetic flux per one cell (of the area S) of the array is an integer number $m = 0, \pm1, \pm2, \ldots$ of the magnetic flux quanta. We note a somewhat more complicated (although rather symmetric with respect to the origin) structure of the peaks with $m > 1$ which can be due to magnetic field penetration into overlapping parts of Nb and Pb films forming each cell and into the junctions themselves.

Although Fig. 2(a) and Fig. 2(b) show qualitatively the same behavior, there is a quantitative difference between them. With respect to the maximum I_c at $H = H_m$, the relative level of the critical current between the maxima in Fig. 2(b) is lower than in Fig. 2(a). For a multicontact interferometer it is known[10] that the average level of the critical current between the maxima depends upon the SQUID parameter β_L introduced above. When β_L increases above unity this level substantially grows; since $\beta_L \sim I_c$, these data are consistent with the decrease of I_c at higher temperatures. The similar behavior was observed for the 20-junction arrays.

C. Zero-field steps

Here, we present and discuss the results obtained at $H \approx 0$. At $T = 4.2$ K we did not observe any current singularities in the *I-V* characteristic of 1D arrays that we could attribute to fluxon shuttling oscillations. In general, increasing the temperature leads to a decrease of the parameter β_L and to an increase of the losses in the junctions. At temperatures close to the transition temperature of lead, $T_c^{\mathrm{Pb}} \approx 7.2$ K, we observed resonant branches similar to that of fluxon oscillations in long junctions. The *I-V* characteristic at $T = 6.9$ K ($\beta_L \approx 1$) is shown in Fig. 3(a). Due to different critical temperatures of the top and bottom electrodes a nearly linear slope appears at voltages below $(\Delta_{\mathrm{Nb}} - \Delta_{\mathrm{Pb}})/e$. The enlarged *I-V* curve is shown in Fig. 3(b). The step at about 50 μV was stable only in a narrow field range around zero. This is closely reminiscent of the first zero-field-step (ZFS1) resonance of a long Josephson junction and corresponds to a single fluxon performing a shuttle motion in the array. As expected, for $H \neq 0$ we found the low-order Fiske steps (see next subsection) to have a voltage spacing $\Delta V_{\mathrm{FS}} = 0.5\, V_{\mathrm{ZFS1}} \approx 25\ \mu$V. From the voltage V_{ZFS1} of the zero-field step the Swihart velocity of the fluxon moving in the array is estimated to be $\bar{c}_{\mathrm{arr}} = 0.012 c_0$. This is about 4 times smaller than

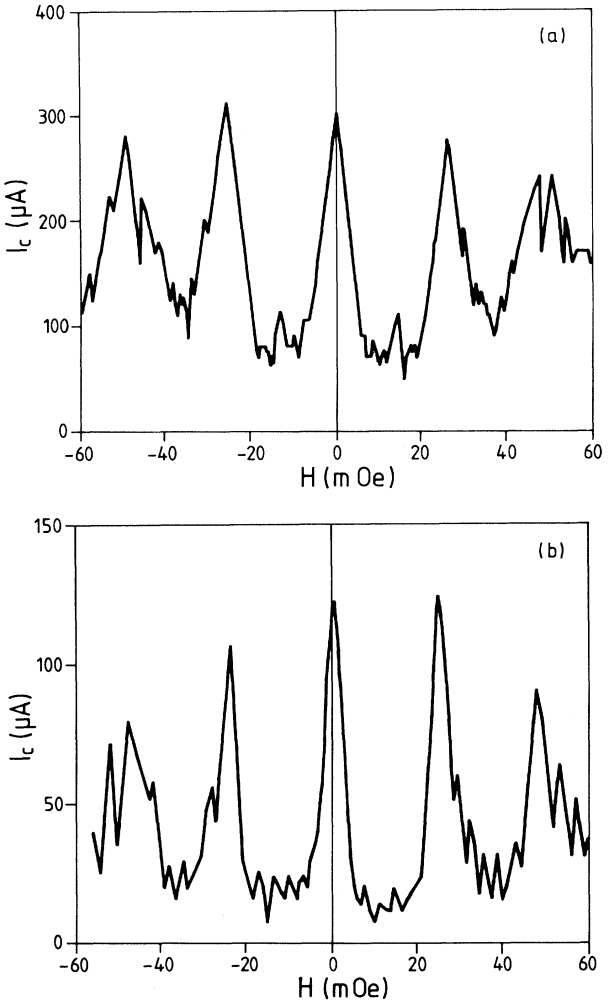

FIG. 2. The dependence of the critical current I_c of the 10 Josephson junction array (sample No. OB1-3B) on the magnetic field H at the temperatures $T = 4.2$ K (a) and $T = 6.9$ K (b).

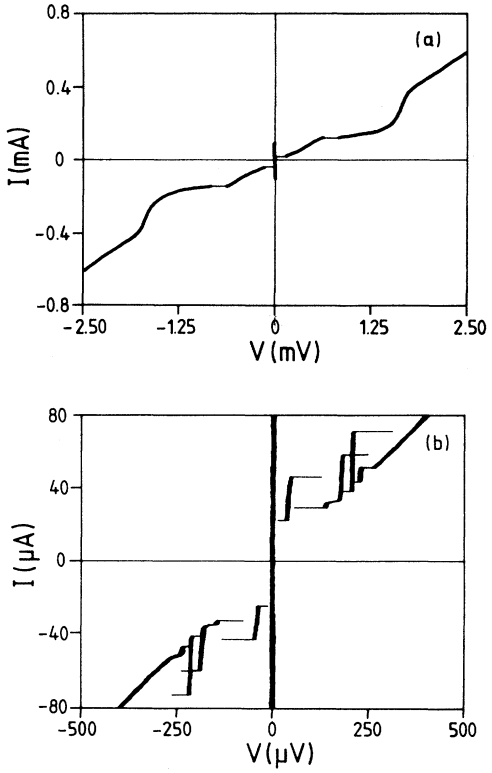

FIG. 3. Current-voltage (I-V) characteristics at $T = 6.9$ K for the 10-Josephson junction array in zero magnetic field (a); on an enlarged scale (b) the first zero-field step is seen at about 50 μV.

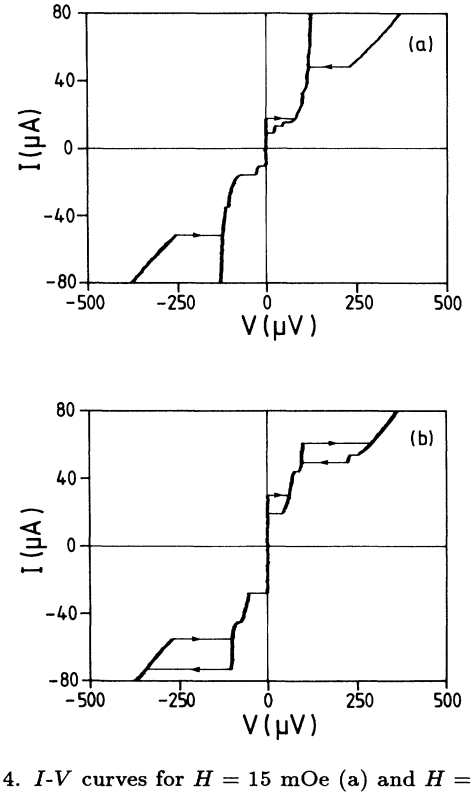

FIG. 4. I-V curves for $H = 15$ mOe (a) and $H = 19$ mOe (b) taken at $T = 6.9$ K which show the resonant flux-flow regime in the 10-junction array.

the Swihart velocity $\bar{c}_{LJJ}$ in the long Josephson junction measured on the same chip.

The higher steps, which are seen in Fig. 3(b) at the voltages 150–250 μV, were found to be very stable around $H \approx 0$. The voltage spacing between them is clearly smaller than V_{ZFS1}. This behavior differs from the high ZFS's in a continuum long Josephson junction, where the voltage spacing between the low and the high zero-field steps remains constant. We suggest that these higher-order ZFS resonances are a fingerprint of the discreteness of the system. As confirmed in Sec. IV by numerical simulations, they are related to the shortest possible wavelength of a standing wave in the array.

D. Flux-flow and Fiske steps

In the temperature range 5.4–7.0 K the application of the external magnetic field H gives rise to flux-flow steps in I-V curves of the arrays. Preliminary, the experimental results which we show in this part have been already presented in Ref. 16. Figure 4 shows the I-V characteristics measured at $T = 6.9$ K for different values of the magnetic field. When increasing the field from 0 to $H_1/2 = 14$ mOe, the voltage V_{FF} of the main flux-flow step increases [Fig. 4(a)]. The explanation for this is that from zero field to the field of $\Phi_0/2$ per cell an increasing number of fluxons (proportional to the applied field) enters the array and performs a unidirectional motion which generates a voltage across the junction. The behavior looks very similar to the flux-flow step in a long Josephson junction. However, at a magnetic field close to $H_1/2$ the flux-flow voltage V_{FF} saturates at about 150–160 μV. When increasing the field further from $H_1/2$ to H_1 the voltage V_{FF} decreases, as seen in Fig. 4(b). A possible interpretation is that for fields larger than $H_1/2$ a fixed number of fluxons which is commensurate with the lattice remains pinned and the most energetically favorable dynamical state is a motion of vacancies in this fluxon chain instead of a motion of all the fluxons themselves. A similar behavior has been observed in long continuous Josephson junctions with a lattice of artificially prepared inhomogeneities[15] and in overdamped 1D Josephson junction arrays.[14] As the number of vacancies decreases with increasing H from $H_1/2$ to H_1, the step voltage also decreases.

At nonzero field, small steps at about 25 μV and 50 μV are observed along with the flux-flow step, as shown in Fig. 4(a). The asymptotic voltages of these steps, within a 15% accuracy, are half-multiples of the voltage V_{ZFS1} of the zero-field step at $H \approx 0$ shown in Fig. 3(b). We see in Fig. 4 that the upper part of the flux-flow step is split into several close resonances. The voltage spacing between these resonant steps is clearly smaller than the voltage spacing between the low-order Fiske steps. The voltage position of various fine structure steps in the flux-flow I-V characteristics at the field range $0 < H < H_1$ is

summarized in Fig. 5. Here the first Fiske step and the second Fiske step (which coincides with ZFS1 at $H \approx 0$) are clearly noticeable at approximately constant voltage levels of about 25 μV and 50 μV. At high voltages the distribution of steps looks rather complicated and the voltage spacing between them is reduced. Except for the zero-field range, this picture is very similar to that observed by van der Zant *et al.*[7] They also found the saturation of maximum step voltages together with squeezing of the voltage spacing between high steps and interpreted them as cavity resonances on the discrete lattice. As discussed further in Sec. IV, the spacing between high Fiske steps (HFS's) is decreasing due to the flattening of the dispersion relation for linearized waves in the discrete array for wave vectors approaching π/a. We would like to emphasize that the high zero-field steps (HZFS's) reported in the previous subsection are essentially *different* from the high-order Fiske steps described here and also analyzed in Ref. 7. HZFS's appear at voltages above 160-180 μV and they are separated from the lower ZFS's by an instability region on the *I-V* curve [at 60–150 μV in Fig. 3(b)]. HFS's are always seen at voltages below 160 μV and they are parts of the flux-flow branch which is separated from the high-voltage linear slope (McCumber line) by the same instability region [at 160–220 μV in Fig. 4(b)]. For field values ranging in the interval $H_m < H < H_m + H_1/2$ [like in Fig. 4(b) for $I > 0$] HZFS's and HFS's coexist, but we never observed any HZFS's at $H \approx H_m + H_1/2$ (where HFS's are mostly dominating) or any HFS's at $H \approx 0$ (where ZFS's and HZFS's are observed).

At the temperatures close to T_c^{Pb}, the 20-junction arrays showed behavior similar to that of the 10-junction arrays. The flux-flow step reached approximately the same maximum voltage of about 150 μV for the field close to $H_1/2$. As expected from the fluxon propagation model for long junctions, the flux-flow voltage depends only on the density of fluxons and their velocity in the array, and it does not depend on the length of the system. In contrast, the Fiske step voltage spacing (which is expected to be inversely proportional to the length of the system) was found to be roughly a factor of 2 smaller than that of the 10-junction array.

For magnetic fields $H > H_1$ a very similar flux-flow behavior to that at $0 < H < H_1$ has been found. The flux-flow steps were observed between the peaks of the critical current I_c at $H = H_m$. For $H \approx H_m$ and $m > 1$ we did not find any steps at higher voltages (neither the lower ZFS's nor HZFS's). One possible reason for this effect is that the high I_c peaks in Fig. 2 look rather complicated, probably due to nonlinearity of cell inductances and the field penetration into the junctions.

The typical *I-V* characteristics of the 10-junction array in the lower-temperature range (5.0–5.5 K) are shown in Fig. 6(a). In a magnetic field $H_{\mathrm{FF}} \sim 13$ mOe a linear resistive branch is observed in the current-voltage characteristic. In a limited field range (about ± 1 mOe around H_{FF}) the voltage of this structure was found to depend linearly on H: The increase of H led to a shift of the whole step to the right along the voltage axis. This step was always observed to be very smooth, and no fine structure resonances in this regime have been found. The *I-V* characteristic at the same value of H but for slightly higher temperature $T = 5.7$ K is shown in Fig. 6(b). We clearly observe that with *increasing the temperature* the resistive branch evolves into current singularities. It is essential to note that this behavior is just the oppo-

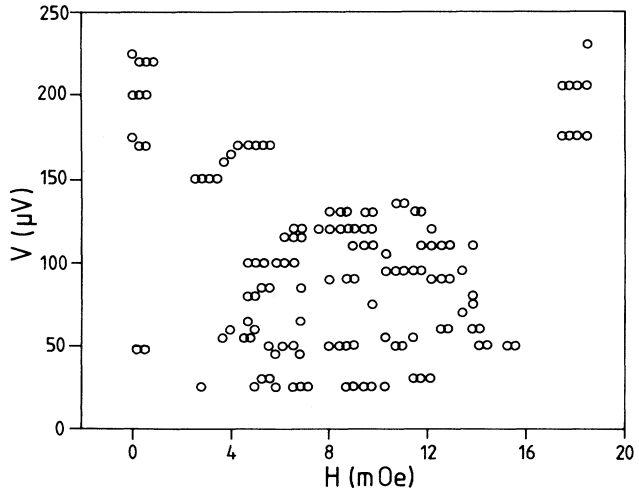

FIG. 5. Asymptotic step voltages as function of magnetic field H, at $T = 6.9$ K (sample No. OB1-3B).

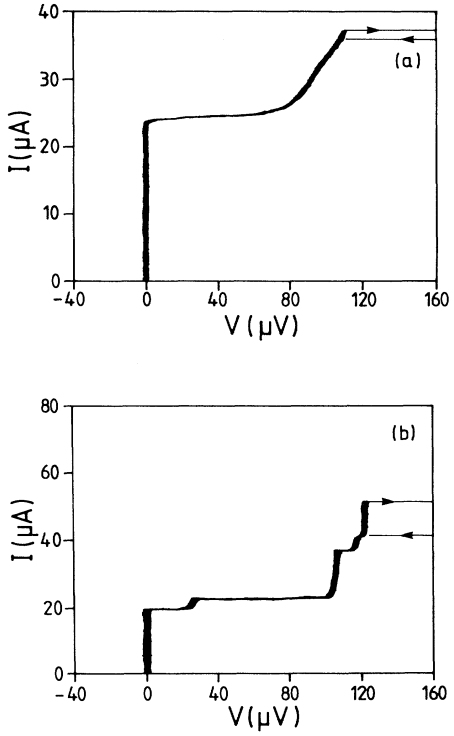

FIG. 6. *I-V* curves of the 10-junction array at $H = 13$ mOe for $T = 5.04$ K (a) and $T = 5.04$ K (b). The curves show the linear flux-flow branch (a) which evolves into a resonantlike structure (b) with *increasing the temperature.*

site to that of a conventional long Josephson junction, where resonant steps (zero-field steps and Fiske steps) become much more pronounced with decreasing the temperature. For a Josephson junction in general, increasing the temperature leads to a decreasing of the quasiparticle resistance and therefore to higher damping. Increasing the temperature, the steps in long junctions become less steep because of the increasing losses experienced by moving fluxons. The crossover between Fig. 6(a) and Fig. 6(b) shows just the opposite: *In discrete arrays the increase of damping leads to the splitting of the linear flux-flow branch into several sharp resonantlike steps.*

III. MODELING AND SIMULATIONS

A 1D parallel array of Josephson junctions can be described by the discretized version of the perturbed sine-Gordon equation

$$\frac{d^2\varphi_n}{dt^2} + \alpha\frac{d\varphi_n}{dt} + \sin\varphi_n + \gamma - \frac{1}{a^2}(\varphi_{n-1} - 2\varphi_n + \varphi_{n+1}) = 0\,, \quad (1)$$

where $1 \le n \le N+1$, $N+1$ is the number of junctions, and φ_n is the superconducting phase difference on the nth junction. In order to simplify the comparison with the continuum case all the parameters in Eqs. (1) are written in the standard notation used for a long Josephson junctions:[1] The spatial coordinate x is normalized to the effective Josephson penetration depth $\lambda_J = D/a$ (D is the spatial interval occupied by a single cell of the array, and a is the discreteness parameter introduced in Sec. II), the time t is normalized to the inverse plasma frequency $\omega_0^{-1} = [\Phi_0 C/J_c]^{1/2}$, C is the averaged capacitance per unit length of the array, $\alpha \sim 1/R_n$ is the dissipation coefficient, and γ is the spatial averaged bias current density normalized to the spatially averaged critical current density $J_c = (N+1)I_c/(DN)$. The equivalent circuit described by Equation (1) is shown in Fig. 1(b). Eq. (1) is written in the simplest approximation where all mutual inductances between different cells in the array are neglected. A complete (and more complicated) treatment of this problem with long-range mutual inductances included has been performed recently by Bock *et al.*[17] van der Zant *et al.*[7] analyzed their experimental results on 1D arrays using the models with self-inductance only and with nearest-neighbor inductance included. They concluded that the effects of the nearest-neighbor inductances M play a rather important role and obtained the best fit of their data by taking $M/L_0 = 0.12$–0.16. In the present work we keep our approach simple and focus on several qualitative features in the behavior of underdamped 1D arrays. Thus, in the following we only consider the model (1).

In the limit of $a \to 0$ the model (1) corresponds to the continuum model described by the continuous PSGE.[3] Thus, for a 1D array with small a we might expect a dynamical behavior close to that of a long Josephson junction. This means that in long 1D arrays ($Na \gg 1$) with sufficiently small a dynamic regimes like ZFS, FS, and FFS regimes should appear in the I-V characteristics. The realization of these states depends on the boundary conditions for such an array, which are given by the magnetic field H applied at the boundaries. As a reasonable approximation, the magnetic field in the first and the last cells can be taken equal to the externally applied field:

$$\frac{\varphi_2 - \varphi_1}{a} = \frac{\varphi_{N+1} - \varphi_N}{a} = h\,, \quad (2)$$

where $h = H/(\lambda_J J_c)$ is written in the standard notation used for long Josephson junctions. Typically, for long Josephson junctions the ZFS regime is observed for $h \sim 0$, the FS regime for $h \sim 1$, and that of the FFS for $h > 2$. For the open ($h = 0$) boundary conditions, the oscillations of a single fluxon correspond to the first zero-field step (ZFS1) on the I-V characteristics. The fluxon is expected to perform a shuttlelike motion in the array and to reverse its polarity at any collision with a boundary.

When a is of the order of the unity or greater, the discreteness effects become important. In general, the kink motion through a discrete lattice leads to radiation of small-amplitude linear waves.[4] With $\alpha = \gamma = 0$, Eq. (1) corresponds to the well-known Frenkel-Kontorova model. The dispersion relation for linear waves, $\varphi_n = \varphi^{(0)}\exp[i(\omega t - kan)]$, is known to be

$$\omega^2 = 1 + \frac{4}{a^2}\sin^2\left(\frac{ka}{2}\right)\,, \quad (3)$$

where ω is the frequency of the linear waves (lattice phonons) and k is their wave number. van der Zant *et al.*[7] studied the Fiske modes in a relatively short 1D arrays with rather small discreteness $a < 0.5$ and showed that the voltages of resonant steps observed in I-V characteristics nicely picture the dispersion relation (3). In that case Fiske steps are essentially cavity resonances in the applied magnetic field which can be understood in the framework of the linear model. In the longer arrays studied here, due to a nonlinearity which characterizes the motion of kinks (fluxons), the whole behavior is more complicated. From pure kinematics, a resonance between the emitted waves and the moving periodic chain of fluxons can occur when the phase velocity of the excited linear waves coincides with the fluxon velocity. Imposing further that the period of the linear waves and the period of the fluxon chain must commensurate, a resonance condition can be obtained for fluxon steps.[6]

In order to understand our experimental results in the framework of the discrete sine-Gordon model discussed above, we performed numerical simulations of the system of Eqs. (1) and (2) for an array consisting of ten cells. The integration was made using a fourth-order Runge-Kutta scheme with the time step equal to 0.02 or 0.05. In order to see the hysteresis between the steps, the current γ was swept up and then down. In each sequential point of the I-V curve the initial conditions were taken from the stationary state achieved in the previous point. In order to eliminate the transient due to the change in γ in each point, the voltage integration was performed over a long time interval (up to 3000 normalized time units for low

α). In the numerically calculated I-V curves the voltage v is normalized to the asymptotic voltage of the first Fiske steps of the continuum junction. For experimentally studied 10-junction array, one unit of v corresponds to a voltage of $\Delta V_{\rm FS} \approx 25\ \mu$V.

Our experimental estimates for the discreteness parameter a is $a \approx 1.0$ at $T = 4.2$ K and $a \approx 0.6$ at $T = 6.9$ K. From previous numerical simulations[6] made for a=0.2–2.5 with $\alpha = 0.1$ one learns that in this range of a there is no strong change in the system behavior. Fluxons can propagate in the system and the I-V curve should display resonancelike steps due to their motion. On the other hand, in experiments the dissipation parameter α changes from $\alpha \approx 0.02$ at $T = 4.2$ K to $\alpha \approx 0.2$ at $T = 6.9$ K. In order to study the influence of the pure change of the dissipation α on the array properties [in relation with the crossover from Fig. 6(a) to Fig. 6(b) found experimentally] we performed numerical simulations with a fixed discreteness parameter $a = 1$ and varied α from 0.02 to 0.2.

A. $\gamma_c(h)$ dependence

Figure 7 shows the calculated dependence of the critical current density γ_c vs the normalized magnetic field h for an array of ten cells with the discreteness parameter $a = 1$. In normalized units, for $a = 1$ the magnetic field corresponding to one flux quanta per cell is $h = 2\pi$. This $\gamma_c(h)$ curve qualitatively agrees with the experimental behavior shown in Fig. 2.

B. Zero-field I-V characteristics (high damping)

Figure 8(a) shows the first quadrant of the calculated I-V curve of the array for $h = 0$. In agreement with the experimental data shown in Fig. 3, the numerical simulations indicate the resonant zero-field steps. The lowest step (ZFS1) at $v \approx 1$ corresponds to a single fluxon oscillating in the array, the second step (ZFS2) accounts for two oscillating fluxons, etc. As in the experiment, we note that the voltage spacing between the neighboring high-order steps is clearly smaller than the voltage of the lowest ZFS's. For ZFS1, on a detailed voltage scale shown in Fig. 8(b) one can clearly see the fine structure investigated before in Refs. 6, 19 which is due to the resonances between the moving fluxon and its radiation induced by the array discreteness. The fine structure becomes even more pronounced for the higher steps from ZFS2 to ZFS4.

In order to understand the magnetic flux dynamics corresponding to different zero-field steps, we have investigated the spatiotemporal phase patterns of different dynamic regimes. In a quasicontinuum approximation, we plotted the spatial and time dependences of the points where $\varphi(x,t) = 2\pi j + \pi$, with j being an arbitrary integer. These points approximately correspond to the locations of the fluxon centers of mass in the array. For the point

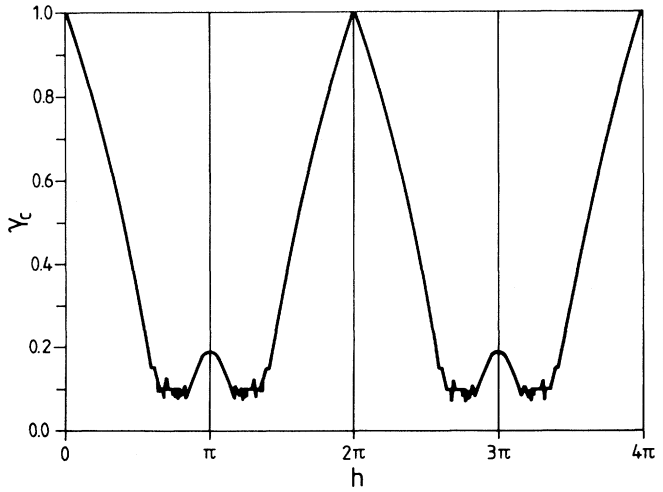

FIG. 7. The calculated dependence of the critical current density γ_c vs the normalized magnetic field h for an array of ten cells with the discreteness parameter $a = 1.0$.

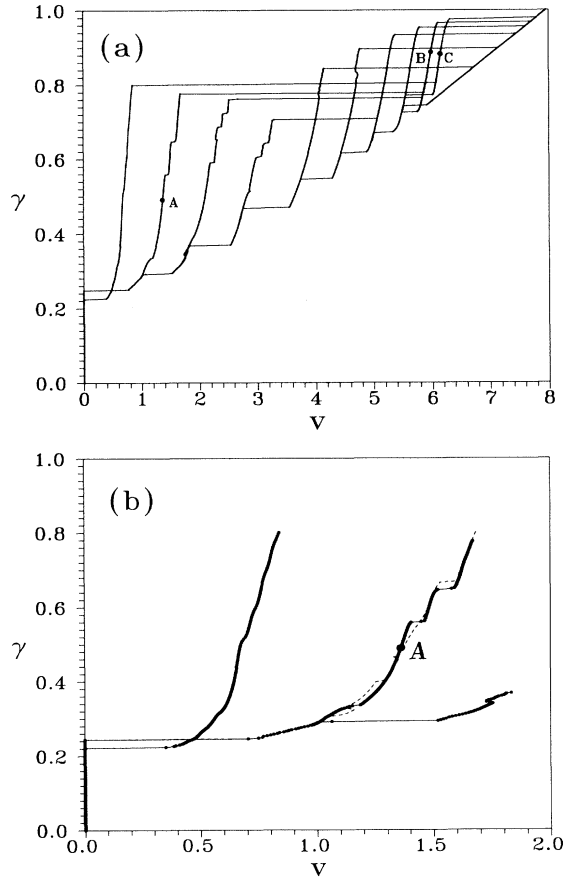

FIG. 8. Numerically calculated I-V curves in zero magnetic field of 1D array of ten cells with $\alpha = 0.2$ and $a = 1.0$: (a) full voltage range with resonant steps; (b) the first two steps (ZFS1 and ZFS2) with enlarged voltage scale. The dashed line shows another stable solution (with bunched fluxons) for ZFS2 obtained using different initial conditions at the starting point of the simulations ($\gamma = 0.4$).

A at ZFS2 in Fig. 8(a), depending on the initial conditions in the simulations, we found several stable regimes exhibiting slightly different average voltages. Two such patterns $\varphi(x,t)$ are shown in Figs. 9(a) and 9(b). Each line corresponds to a fluxon trajectory and its slope gives the fluxon velocity. We find both the symmetric and the asymmetric (bunched) dynamic fluxon states. The full I-V characteristics of these states are shown in Fig. 8(b) by the solid and the dashed lines on ZFS2, respectively. The reason for the two-fluxon bunching in discrete 1D arrays is the radiation of the linear waves emitted by the first (leading) fluxon and its interaction with the next coming fluxon(s). The emitted waves have phase velocity equal to the fluxon velocity.[6] A bunched state becomes stable if the second fluxon meets the oscillation excited by the first fluxon in phase.

The dynamic regimes for two of the high steps corresponding to the points B and C in Fig. 8 are shown in Figs. 9(c) and 9(d). For these regimes the phase trajectories indicate the dynamic states which correspond to cavity resonances on the discrete 1D lattice. The highest ZFS10 [Fig. 9(d)] corresponds to the smallest possible wavelength equal to $2a$ in the discrete lattice. This can be associated with one-dimensional phonon-type excitations at the end of the Brillouin band. The cavity resonances are equidistant in the wave number k space and the step voltage is proportional to their frequency ω. As illustrated in Fig. 10, the nonlinear dispersion relation for a discrete lattice (3) leads to the squeezing of the frequency intervals (which is proportional to the voltage spacings) between the high-order steps, as observed here in experiment and numerical simulations. For ZFS9 the *average wavelength* of the cavity mode is $2a \times 10/9$, for ZFS8 it is $2a \times 10/8$, and so on for the lower steps. However,

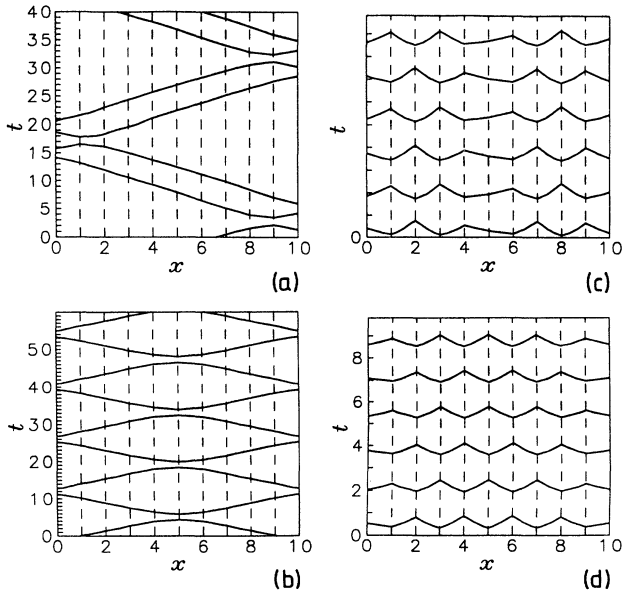

FIG. 9. Phase trajectories in different points of the calculated I-V curve shown in Fig. 8: Both (a) and (b) correspond to point A, (c) point B, (d) point C.

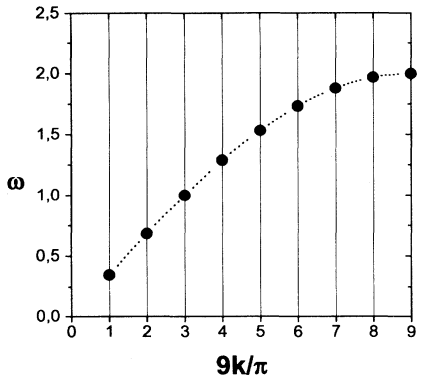

FIG. 10. Illustration of the frequency positions of the cavity resonances based on the dispersion relation (3) with $a = 1.0$.

the *local wavelength* can be different from the average one, as at $x = 5$ in Fig. 9(c). As seen in Fig. 8(a), the high ZFS's corresponding to the cavity resonances are very straight without any pronounced fine structure. In contrast, intermediate steps like ZFS3 and ZFS4 display a rich structure which can be due to the competition between the fluxon propagation mode and the cavity resonances in the 1D array. This competition can be the reason for poor stability of the intermediate ZFS's. This may explain why we did not observe these steps in the experiment; they should appear in the instability range discussed in Sec. III.

C. Flux flow at a finite field: Low damping

Figure 11(a) shows the calculated current-voltage (I-V) characteristics of the array with $\alpha = 0.02$ for $h = 2.1$ and $h = 3$. In normalized units, for $a = 1$ the magnetic field h corresponding to $H \sim H_1/2$ (with the average magnetic flux $\Phi_{av} = \Phi_0/2$ per cell) is $h = \pi$. Thus, it is appropriate to compare the calculated curves for $h \sim 3$ with the experimental data shown in Fig. 6(a). One can see that, in qualitative agreement with experiment, the numerical simulations indicate around $v = 3$ an almost linear slope in the I-V curves. We did not find sharp resonant steps in any I-V characteristics calculated with various h values for $\alpha = 0.02$ using integration times up to 6000 time units. Moreover, detailed study of the time-dependent voltage in several bias points showed features of chaotic dynamics with an almost flat Fourier spectrum. In agreement with the experimental observations, Fig. 11(a) shows that changing the magnetic field h moves the linear branch along the voltage axis.

D. Flux flow at a finite field: High damping

In contrast to the low damping behavior described above, for sufficiently high damping $\alpha = 0.2$ we find clear resonant steps in the calculated I-V curves, as shown in Fig. 11(b). After changing each bias current value, the

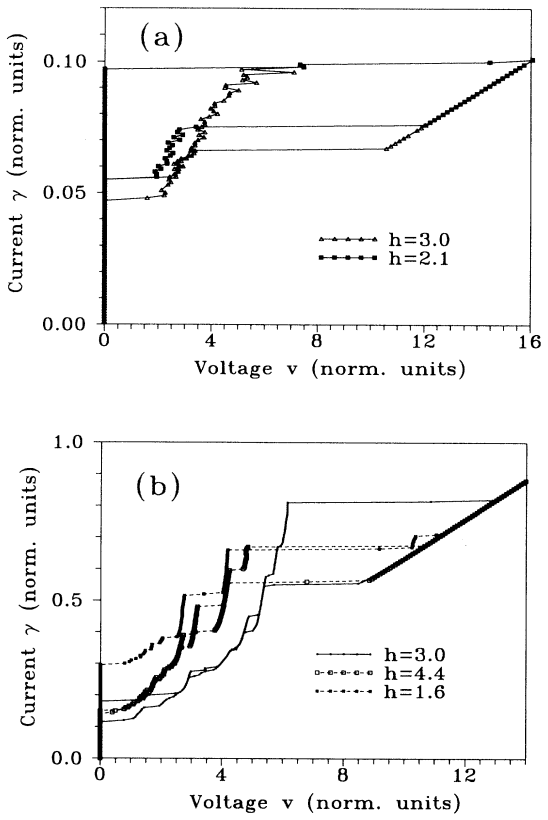

FIG. 11. Numerically calculated I-V curves for $\alpha = 0.02$ (a) and $\alpha = 0.2$ (b) which show the chaotic dynamics (a) and the resonant flux-flow steps (b) in the 10-cell array.

stationary regime was typically achieved within less than 200 time units. The time-dependent voltage in the array showed stable periodic oscillations with several harmonics and subharmonics in the Fourier spectrum, depending on the bias point. In good agreement with experimental data shown in Fig. 4, the calculated I-V characteristics consist of well-separated resonant singularities which all together give rise to a profile similar to that of the flux-flow step in a long Josephson junction. The figure shows the curves calculated for three different values of the normalized magnetic field h: $h = 3.0$ ($\Phi_{\rm av}/\Phi_0 = f \approx 0.5$), $h = 4.4$ ($f > 0.5$), and $h = 1.6$ ($f < 0.5$). In close correspondence with the experimental behavior, increasing h from 0 to about 2.3 the maximum voltage $v_{\rm FF}$ of the highest step is also increasing. In the interval $2.2 < h < 4.0$ the voltage $v_{\rm FF}$ saturates at about 6, which agrees with the experimentally measured saturation at $V_{\rm FF}$ about $6\Delta V_{\rm FS} \approx 150\mu$V. As we see in Fig. 11(b), an increase of h above 4.0 leads to a decrease of $v_{\rm FF}$. As in experiments, for $h \approx 2\pi$ ($H \approx H_1$) the flux-flow step disappears.

IV. DISCUSSION

We find a remarkable number of similarities between the dynamics of one-dimensional parallel arrays of small Josephson junctions and that of a uniform long Josephson junction. As in a long junction, in the I-V characteristics we observe zero-field step, Fiske steps, and flux-flow steps. Furthermore, the numerical simulations furnish strong evidence that the observed singularities are generated by different fluxon dynamical regimes in the discrete system. The discreteness of the system, however, induces phenomena which do not have parallels in the continuous system. The saturation of the flux-flow step voltage in the middle between the magnetic field H_m and H_{m+1} ($m = 0, \pm 1, \pm 2, ...$) where the fluxon array commensurates the underlying lattice is a clear indication of the array discreteness. Moreover, when the flux-flow step is approaching the saturation level the voltage spacing between the high fine structure resonances (which are expected to be the analog of the Fiske steps in the discrete array) is noticeably decreasing. This effect has been found both in experiment [Fig. 4(a)] and in numerical simulations [Fig. 11(b)].

From the voltage position of the zero-field step and the lower Fiske steps the experimental value for the Swihart velocity has been estimated as $\bar{c}_{\rm arr} = 0.012c_0$. For a long overlap junction ($L = 100$ μm) on the same chip we found a zero-field step at $V = 320$ μV which yields the Swihart velocity of $\bar{c}_{\rm LJJ} = 0.05c_0$. In a long junction the Swihart velocity is known to be the propagation velocity of electromagnetic waves through a transmission line with a given capacitance and inductance per unit length. A natural way of estimating the expected Swihart velocity for the discrete array is to use the average capacitance and inductance per length. Thus, in order to evaluate $\bar{c}_{\rm arr}$ for the discrete line we take the capacitance of the small junctions divided by the length of the array, and the inductance of a single cell divided by the length of the cell. A rough estimate of the cell inductance can be made using the Jaycox-Ketchen formula for a square hole in an infinite film of superconductor.[18] A value of 10pH is found for a loop area of ≈ 40 μm^2. Using this simple approach the predicted value of the zero-field step is found to be $V_{\rm ZFS} = 170$ μV, i.e., about 3 times larger than the experimental value. A better estimate of the loop inductance can be made using the formula for a square washer of finite dimensions.[20] This gives an inductance of 88 pH with a prediction of ZFS1 asymptotic voltage $V_{\rm ZFS} = 58$ μV in better agreement with the actually measured value of about 50 μV.

Mutual inductance effects, which are not included in our model, could have a substantial influence on the effective inductance per one cell of the array. Also, for our estimation we take the maximum measured voltage on the step as the Swihart velocity voltage, whereas the true asymptotic voltage should be somewhat higher. We note that numerical simulations[6] of the single-fluxon I-V characteristics in the 1D array with $a \sim 1$ show that the asymptotic voltage of the first zero-field step which we measure can be 20%–25% lower than the true value corresponding to the Swihart velocity. The explanation of this phenomenon arises from the simple intuitive argument that the Lorentz-contracted size of a fluxon cannot become smaller than the discreteness of the lattice a. Thus, even for large γ a fluxon in the 1D array cannot

move faster than a certain maximum velocity $\tilde{v}(a) < 1$.

An important effect in the discrete system is the modified dispersion relation for linearized waves. In the continuum sine-Gordon system the dispersion relation is $\omega^2 = 1 + k^2$ and the waves approach a constant group velocity when the wave vector k becomes large. In a discrete system the maximum wave vector inside the Brillouin band is $k = \pi/a$. Furthermore, the dispersion relation (3) is different from that of the continuum case. As schematically shown in Fig. 10, it gives increasingly densely spaced values of ω for equidistantly spaced values of k close to $k = \pi/a$. This fact explains why in the 10-junction array the flux-flow voltage at the field corresponding to $\Phi_0/2$ per cell ($h \sim \pi$) does not reach $5V_{\mathrm{ZFS1}}$ as is expected in a long Josephson junction. In the array, the tenth Fiske step (FS10) appears at a voltage significantly smaller than $5V_{\mathrm{ZFS1}}$. The experimentally found ratio $V_{\mathrm{FS10}}/(5V_{\mathrm{ZFS1}}) \approx 0.6$ is in good agreement with the theoretical expectation $2/\pi \approx 0.64$.

An alternative model for the HFS's could be the resonances between fluxons moving in the discrete system and the linear waves radiated by them. Such an effect has been found numerically for an annular array with a single fluxon circulating in it.[6] However, this approach is relevant in quasicontinuum approximation, i.e., when the kink size and the spacing between the kinks (fluxons) is much larger than the lattice spacing a. This is not the case for $H \sim H_1/2$ where the fluxon spacing is about $2a$.

For future studies it might be interesting to investigate the relative stability and the competition between different types of resonances (low ZFS's, HZFS's, HFS's) in the system. Here we only note that there is an instability region between the lower ZFS's and the HZFS's, which strongly depends on the dissipation α and the discreteness parameter a. In the numerical simulations we did not introduce any noise in the system which might be essential for a relevant comparison with experiment. Another interesting problem to look at is the scenario of the transition to a chaotic dynamical state (linear flux-flow branches at lower temperatures) as a function of α and a.

We want to emphasize that the chaotic state that we have found in numerical simulations appears without any external ac current drive. The existence of spatial chaos in the discrete sine-Gordon system for the static case has been demonstrated recently.[21] It is worth noting that the linear branches in Fig. 6(a) and Fig. 11(a) are reminiscent of those observed in long Josephson junctions for different current and magnetic field biasing conditions.[22] We suggest that there is a general reason for such behavior. Due to the nonintegrability of the discrete sine-Gordon model different modes (kinks and small oscillations) are always present in the system. With decreasing the damping (temperature in our array experiment) the competition between these modes causes an increase of the intrinsic noise and, finally, a transition to a chaotic dynamic state. At low temperatures (which corresponds to very small damping accompanied by substantially increased discreteness of the arrays) no stable fluxon dynamic regions have been found in the I-V characteristics.

V. SUMMARY

We reported here experiments and numerical simulations of fluxon dynamics in one-dimensional parallel arrays of small underdamped Josephson tunnel junctions. Experimental data on fluxon propagation in arrays are compared with that for continuous junctions made on the same chip. The current-voltage characteristics of the arrays show various resonant steps corresponding to the fluxon oscillations. In particular, here we observed a zero-field step corresponding to a single fluxon shuttling in the array. Our experimental data supported by numerical simulations suggest that the concept of a fluxon as a moving relativistic particle can be still used even for strongly discrete lines. In the shortest-wavelength limit (determined by the line discreteness) we find new features in the dynamic behavior which do not exist in the continuum case.

The most prominent feature of discrete arrays is the squeezing of the voltage spacing between high-order resonant steps in I-V characteristics. In addition to the squeezed high-order Fiske steps (which appear at the top of the flux-flow branch starting from zero voltage) previously reported by van der Zant *et al.*,[7] we observed also high-order squeezed zero-field steps (which appear at the bottom of the linear McCumber slope). Our numerical simulations show a rather simple qualitative model which explains the physical mechanism for these resonances as due to cavity waves in a discrete line.

Measurements have been performed at different temperatures which allowed us to vary the damping and the effective discreteness in the arrays. At high temperatures the I-V curves display most of the characteristic regimes usually associated with long continuum underdamped Josephson junctions, although with a somewhat more complicated structure of the resonant steps. Decreasing the temperature these steps cause them to evolve into smaller and more linearlike branches which can be tuned by H. At low temperatures (which correspond to very small damping accompanied by a substantially increased discreteness of the arrays) no fluxon dynamic regimes have been found in the I-V characteristics. We note that substantial damping is needed in a real system to stabilize kink propagation through the discrete lattice; otherwise a transition to a chaotic regime is observed.

ACKNOWLEDGMENTS

We thank V. Merlo for helping us in setting up the experiment and R. Leoni for design advice. We thank G. Costabile, Yu. S. Kivshar, B. A. Malomed, T. P. Orlando, S. Pagano, R. D. Parmentier, M. Peyrard, and H. S. J. van der Zant for valuable discussions. Special thanks are due to Professor Ivo Modena for his support, advice, and encouragement. The partial financial support of this work by the Progetto Finalizzato *Tecnologie Superconduttive e Criogeniche* of CNR (Italy) is acknowledged. A.V.U. and B.H.L. would like to thank the Dipartimento di Fisica, Universita' di Roma "Tor Vergata" for the kind hospitality. B.H.L. acknowledges partial financial support from the Otto Mønsteds Fond.

* Permanent address: Institute for Thin Films and Ion Technology, Research Center (KFA), D-52425 Jülich, Germany.
† Permanent address: Physics Department, Technical University of Denmark, DK-2800 Lyngby, Denmark.
‡ Permanent address: Institute of Solid State Physics, Russian Academy of Sciences, Chernogolovka, Moscow district, 142432, Russia.
§ Permanent address: Dipartimento di Energetica, Università degli Studi di L'Aquila, L'Aquila, Italy.

[1] R. D. Parmentier, in *The New Superconducting Electronics*, edited by H. Weinstock and R. W. Ralston (Kluwer Academic Publishers, Dordrecht, 1993), p. 221; see also N. F. Pedersen, in *Solitons, Modern Problems in Condensed Matter Sciences*, edited by A. A. Maradudin and V. M. Agranovich (North-Holland, Amsterdam, 1986), p. 486.
[2] M. Cirillo, R. D. Parmentier, and B. Savo, Physica D **3**, 565 (1981).
[3] D. W. McLaughlin and A. C. Scott, Phys. Rev. A **18**, 1652 (1978).
[4] M. Peyrard and M. D. Kruskal, Physica D **14**, 88 (1984).
[5] G. Costabile and P. Sabatino, in *Future Directions of Nonlinear Dynamics in Physical and Biological Systems*, edited by P. L. Christiansen, J. C. Eilbeck, and R. D. Parmentier, Vol. 312 of *NATO Advanced Study Institute, Series B: Physics* (Plenum, New York, 1993), pp. 339–342; G. Rotoli, *ibid.*, pp. 363–366.
[6] A. V. Ustinov, M. Cirillo, and B. A. Malomed, Phys. Rev. B **47**, 8357 (1993).
[7] H. S. J. van der Zant, D. Berman, T. P. Orlando, and K. A. Delin, Phys. Rev. B **49**, 12 945 (1994).
[8] K. Nakajima, H. Sugahara, A. Fujimaki, and Y. Sawada, J. Appl. Phys. **66**, 949 (1989).
[9] K. K. Likharev and V. K. Semenov, IEEE Trans. Appl. Supercond. **AS-1**, 3 (1991).
[10] J. H. Miller, Jr., G. H. Gunaratne, J. Huang, and T. D. Golding, Appl. Phys. Lett. **59**, 3330 (1991).
[11] G. K. G. Hohenwarter, J. S. Martens, D. P. McGinnis, J. B. Beyer, J. E. Nordman, and D. S. Ginley, IEEE Trans. Magn. **MAG-25**, 954 (1989).
[12] K. K. Likharev, Sov. Phys. JETP **34**, 906 (1972).
[13] S. Hontsu and J. Ishii, J. Appl. Phys. **63**, 2021 (1988).
[14] G. Filatrella, S. Matarazzo, and S. Pagano, in *Future Directions of Nonlinear Dynamics in Physical and Biological Systems* (Ref. 5), pp. 347–350.
[15] V. A. Oboznov and A. V. Ustinov, Phys. Lett. A **139**, 481 (1989).
[16] M. Cirillo, B. H. Larsen, A. V. Ustinov, V. Merlo, V. A. Oboznov, and R. Leoni, Phys. Lett. A **183**, 383 (1993).
[17] R. D. Bock, J. R. Phillips, H. S. J. van der Zant, and T. P. Orlando, Phys. Rev. B **49**, 10 009 (1994).
[18] J. M. Jaycox and M. B. Ketchen, IEEE Trans. Magn. **MAG-17**, 400 (1981).
[19] A. V. Ustinov, M. Cirillo, B. A. Malomed, and Yu. S. Kivshar, Physica B **194-196**, 1765 (1994).
[20] M. B. Ketchen, J. Appl. Phys. **58**, 4322 (1985).
[21] A. T. Filippov and Yu. S. Gal'pern, Phys. Lett. A **172**, 471 (1993).
[22] A. C. Scott and W. J. Johnson, Appl. Phys. Lett. **14**, 316 (1969); A. Barone, J. Appl. Phys. **42**, 2747 (1971); S. Pace and U. Gambardella, J. Low Temp. Phys. **62**, 197 (1986).